

Adaptive Control and Power Management in a Microgrid by using Distribution Grids

C. Ganesh*, C. H. Lenin Babu and K. Pavan Kumar

Department of EEE, Annamacharya Institute of Technology and Sciences, Rajampet, Kadapa - 516126, Andhra Pradesh, India; ganesh.challa@gmail.com, ch.leninbabu@gmail.com, pavankumar0233@gmail.com

Abstract

This project gives a microgrid made up of distinctive Distributed Generation (DG) models that are connected with the submission lines. A vitality administration model is connected to arrange the highlights of the distinctive DG models in the microgrid for framework associated and islanded highlights. This paper proposed microgrid have PV array as a DG unit. Since power generated by a PV array is not constant. In order to maintain stability of grid a proton exchange membrane fuel cell is used to support the grid. The outline is affirmed through different test circumstances to demonstrate the utilitarian capacity of the recommended microgrid, and the procured results are said. Kalman filters are used to extract the harmonic component of distorted source voltage and load current and to generate the necessary references for the controller. In larger power system causes steady state and transient problems. In order to conquer these problems a new Model Predictive Control (MPC) is used.

Keywords: Distributed Generation (DG), Power Management, Microgrid, Photovoltaic (PV), Kalman Filters, Model Predictive Control (MPC).

1. Introduction

In this project, a microgrid made up of a Photo Voltaic or (PV) range, Proton Exchange Membrane Fuel Cell (PEMFC) also known as polymer electrolyte membrane fuel cells and Li-ion Battery or LIB is approved. Lithium-ion Batteries have the best energy density not only per unit weight but also per unit volume. The PEMFC is promoted as a move under constructor unit to require for the vitality created by the sporadic qualities of the PV range.

A micro grid is an alongside acquisition of power inception, strength space for capacity and grant that frequently capacities joined with regular focal lines. This anchor-man of general add with the macrogrid can be killed. The microgrid can then work self sufficiently. From the viewpoint of the lines proprietor, a connected microgrid can be overseen as thought it were one endeavor¹⁻³.

This project gives a far reaching solution for the capacity of a microgrid which will in the meantime conveyance genuine and sensitive energy amid both network associated and islanded capacities, compensate for harmonics in the load voltages, and execute ideal cutting and burden losing under distinctive working circumstances.

2. System Information and Modeling

2.1 System Information

Figure 1 uncovers the settings of the microgrid recommended in this wander that is created to capacity either in the lattice associated or islanded technique. The essential DG gadget comprises of a 40-kW PV mixture⁴ and a 15 KW polymer electrolyte membrane fuel cell or PEMFC, which are allied in side by side to the dc sideward of the

*Author for correspondence

distributed generation inverter1 buttoned up dc-dc boost or step up converters to monitor the dc channel voltage of the dispersed generation inverter at the balanced level by transferred the significant energy. Although there is more than necessary sun ablaze, the photovoltaic design progressed in the paramount energy point tracing method to send maximum dc power.

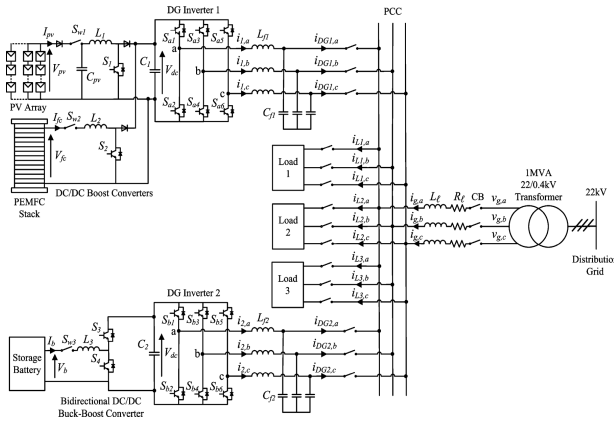


Figure 1. Overall structure of prospective microgrid planning.

MPPT method review making of photovoltaic module and analyzes it to battery voltage later fixed it to the finest voltage to achieve topmost current toward the battery. In addition to supply energy to a dc load this is directly connected to the battery. Amid islanded capacity, the some piece of the storage battery is to engage the vivacity solidness in grid is accustomed by

$$P_{DG} + P_b = P_L \quad (1)$$

Where P_{DG} is the power transferred by the predominant distributed generation unit, P_b is the storage battery energy which is superintend to the charging and releasing restraints accustomed by

$$P_b \leq P_{b,max} \quad (2)$$

P_L is the active power dispatched to the loads. The power restraints of the storage battery are evaluated based on the state of charge boundaries which are given as

$$SOC_{min} < SOC \leq SOC_{max} \quad (3)$$

Although the SOC of battery power cannot be calculated straight, it can be identified through several evaluation methods offered. The SOC of the battery is used to describe the remaining capacity. It is a very important parameter, which reflects the battery performance. The

flowcharts in Figures 2 and 3 review the function of the SB based on the outcome details offered by a Power-Management System (EMS)⁴⁻⁵.

During grid-connected operate, the submission lines is linked with the grid at the PCC through the Circuit Breaker (CB).

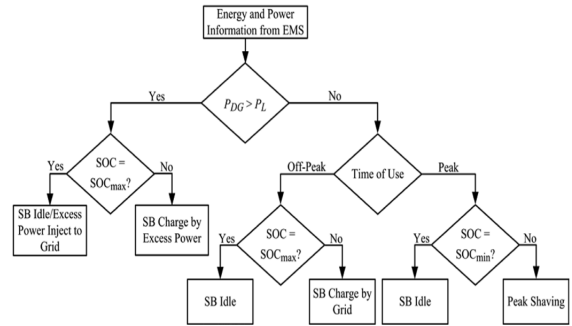


Figure 2. Working of the SB for the period of grid coupled procedure.

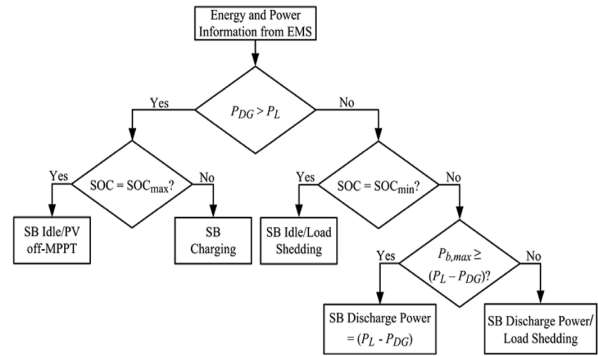


Figure 3. Performance of the SB for the period of islanded procedure.

2.2 DG Inverter Designing

Figures 4 and 5 indicates the commensurable single stage impact of DG inverters for cross section related and islanded limit, exclusively. The turned volts over the consequence of the j th DG inverter is shown by $u_j V_{dcj}$, where u_j is the organization feedback and $j = 1, 2$. The complete weight current i_L which is the aggregate of the voltages sent to the stack ($k = 1, 2, 3$), is given by

$$i_L = \sum_{k=1,2,3} i_{Lk} = i_{L1} + i_{L2} + i_{L3} \quad (4)$$

and can be made as two elements made up of fundamental i_{L_f} and harmonic i_{L_h} with their peak amplitudes I_{L_f} and I_{L_h} respectively, and is showed by

$$\begin{aligned}
 i_L &= i_{Lf} + i_{Ln} = I_{Lf} \sin(\omega t - \varphi_{Lf}) \\
 &+ \sum_{n=3,5,\dots}^N I_{Ln} \sin(h\omega t - \varphi_{Ln}) \\
 &= I_{Lf} \sin \omega t \cos \varphi_{Lf} - I_{Lf} \cos \omega t \sin \varphi_{Lf} \\
 &+ \sum_{n=3,5,\dots}^N I_{Ln} \sin(h\omega t - \varphi_{Ln}) \\
 &= i_{Lf,p} + i_{Lf,q} + i_{Ln}
 \end{aligned} \tag{5}$$

Where φ_{Lf} and φ_{Lh} are the relevant phase angles of the fundamental and harmonic components of i_L . The dispensing grid is delivered by a utility substation described by a voltage source v_g for the period of grid joined task, and is united to the microgrid and the loads via a dispensing line with resistance R_l and inductance L_l .

The DG unit delivers a current i_{DGj} that is given by

$$i_{DGj} = (i_{Lf,p} - i_g) + i_{Lf,q} + i_{Ln} \tag{6}$$

In the matrix associated strategy, the lines volts are known and microgrid offers the heap necessity with the lines. The microgrid will give the general burden prerequisite as demonstrated in Figure 5 and it is required that the result volts be figured out how to an authentic sine pattern with a set size. This can be brought out through the Voltage Control System (VCM).

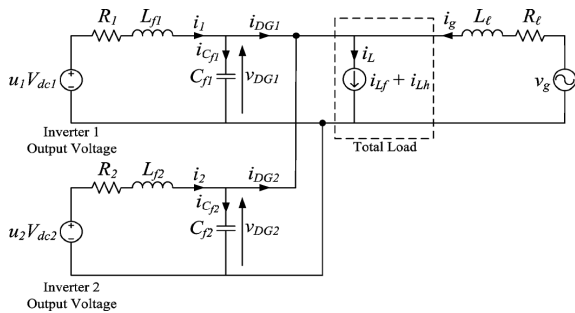


Figure 4. Equivalent single-phase representation of the DG inverters for grid connected operation.

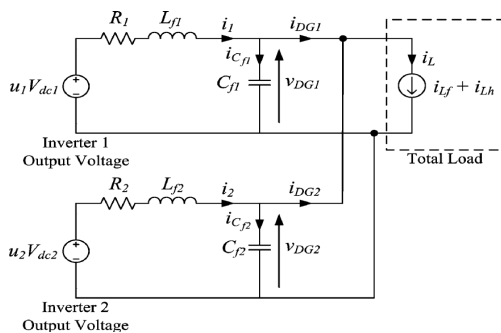


Figure 5. Equivalent single phase representation of the DG inverters for islanded operation.

To procure a state-space plot for the DG inverter in the midst of both cross section related and islanded limits, Kirchhoff's voltage and current laws are activated to the current circuit as presented in Figure 6 and subsequent equations are acquired.

$$\frac{di_j}{dt} = -\frac{R_j}{L_{fj}} i_j - \frac{1}{L_{fj}} v_{DGj} + \frac{V_{dcj}}{L_{fj}} u_j \tag{7}$$

$$\frac{dv_{DGj}}{dt} = \frac{1}{C_{fj}} i_j - \frac{1}{C_{fj}} i_{DGj} \tag{8}$$

Therefore, the grid associated DG inverter model can be presented as

$$x_{gj} = A_{gj} x_{gj} + B_{gj1} v_j + B_{gj2} u_j \tag{9}$$

$$y_{gj} = C_{gj} x_{gj} + D_{gj1} v_j + D_{gj2} u_j \tag{10}$$

Where the subscripts g and j describe the model of distributed generation inverter for the period of grid united operation ($j = 1, 2$) and

$$\begin{aligned}
 A_{gj} &= -\frac{R_j}{L_{fj}}; B_{gj1} = \begin{bmatrix} -\frac{1}{L_{fj}} & 0 \end{bmatrix}; B_{gj2} = \frac{V_{dcj}}{L_{fj}}; C_{gj} = 1 \\
 D_{gj1} &= \begin{bmatrix} 0 & -C_{fj} \end{bmatrix}; D_{gj2} = 0
 \end{aligned}$$

In accordance with the regularity modify details; the EMS will need the primary DG device and the SB to produce the necessary power to fulfill the overall load requirement in the microgrid as proven in the flow-chart of Figure 3. For the time of grid isolated mode performance, the frequency will adjust owed to power imbalance in the microgrid. This change in frequency is detected by the EMS of the microgrid, which is used to control and monitor the power transfer by various DG units. Based on the frequency change notice, the EMS will prescribe the principal distributed generation unit and the Storage battery to generate the necessary power to meet the complete load demand in the microgrid⁵. It proceed from Equation (7) and Equation (8) that DG inverter j can be formed as

$$x_{ij} = A_{ij} x_{ij} + B_{ij1} i'_j + B_{ij2} u_j \tag{11}$$

$$y_{ij} = C_{ij} x_{ij} + D_{ij1} i'_j + D_{ij2} u_j \tag{12}$$

Where the subscript i denotes the model of the DG inverter j during islanded operation ($j = 1, 2$) and

$$A_{ij} = \begin{bmatrix} -\frac{R_j}{L_{fj}} & -\frac{1}{L_{fj}} \\ \frac{1}{C_f} & 0 \end{bmatrix}; B_{ij1} = \begin{bmatrix} 0 \\ -\frac{1}{C_f} \end{bmatrix}; B_{ij2} = \begin{bmatrix} \frac{v_{dcj}}{L_{fj}} \\ 0 \end{bmatrix}$$

$$C_{ij} = \begin{bmatrix} 0 & 1 \\ 1 - \frac{C_{fj}}{C_f} & 0 \end{bmatrix}; D_{ij1} = \begin{bmatrix} 0 \\ \frac{C_{fj}}{C_f} \end{bmatrix}; D_{ij2} = \begin{bmatrix} 0 \\ 0 \end{bmatrix}$$

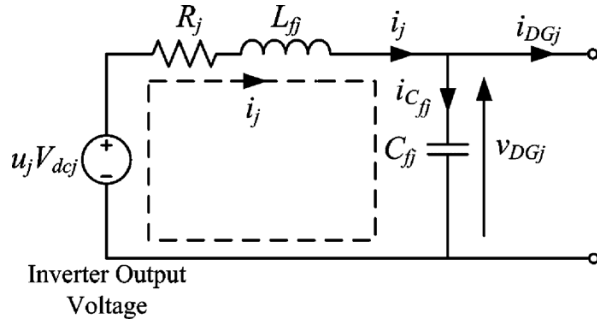


Figure 6. Single phase illustration of the DG inverter for grid united and grid isolated mode operations.

3. Control Design

It is mentioned that in one or other the grid coupled or the grid isolated function, the state space model of portion II-B after making the process of mathematical form,

$$x^+ = Ax + B_1w + B_2u \tag{13}$$

$$y = Cx + D_1w + D_2u \tag{14}$$

Moreover, the antecedent state of this independent model actuates the magnitude and phase angle of this alternate signal. Hence, the exogenous signal ω in Equation (13) and Equation (14) coupled with the reference d that y in Equation (14) desires to track can be developed by,

$$\varepsilon^+ = A_\varepsilon \varepsilon \tag{15}$$

$$\omega = C \omega^\varepsilon \tag{16}$$

$$d = C_d \omega^\varepsilon \tag{17}$$

The exogenous state ξ , and the exogenous kalman filter is represented by,

$$\tilde{\varepsilon}^+ = A_\varepsilon \tilde{\varepsilon} + L_\omega(\omega - \tilde{\omega}) + L_d(d - \tilde{d}) \tag{18}$$

$$\tilde{\omega} = C_\omega \hat{\varepsilon} \tag{19}$$

$$\tilde{d} = C_d \hat{\varepsilon} \tag{20}$$

Where $\tilde{\xi}$ is the predicted exogenous state, and conditions $(\omega - \tilde{\omega})$ and $(d - \tilde{d})$ are actually the difference between the actual ω, d such that $(\omega - \tilde{\omega})$ and $(d - \tilde{d})$ should tend to zero asymptotically. The stable state control u_s and a transient control u_t as,

$$u = u_s + u_t \tag{21}$$

The algorithm dissolves the MPC⁶ optimization into a steady-state sub problem and a transient sub problem, which can be determined in parallel in a receding horizon fashion⁷⁻⁸.

3.1 Stable State Subproblem

The control objective of the stable state subproblem is to analyze an optimal control signal u_s such that when $u \rightarrow u_s$ asymptotically and thus $x \rightarrow x_s$ and $y \rightarrow y_s$ the stable state output y_s should be as close to the desired reference d as accessible. According to Equation (13) and Equation (14), u_s, x_s and y_s should satisfy.

$$x_s^+ = Ax_s + B_1w + B_2u_s \tag{22}$$

$$y_s = Cx_s + D_1w + D_2u_s \tag{23}$$

Subject to the constraints that,

$$|u_s| \leq 1 \tag{24}$$

We deal with the steady state control u_s being developed from a dynamic model predictive control policy approach.

$$\tilde{\varepsilon}^+ = A_\varepsilon \tilde{\varepsilon} \tag{25}$$

$$u_s = c_\varepsilon \tilde{\varepsilon} \tag{26}$$

3.2 Transient State Subproblem

At one time the optimal u_s, x_s and y_s are recognized by the stable state subproblem, the control aim of the transient state subproblem is to certify that the transient signals $u_t = u - u_s, x_t = x - x_s$ and $y_t = y - y_s$ will go to zero immediately. Then according to Equation (13) and Equation (14), and Equation (22) and Equation (23), u_t, x_t and y_t should satisfy,

$$x_t^+ = Ax_t + B_2u_t \tag{27}$$

$$y_t = Cx_t + D_2u_t \tag{28}$$

In this transient state subproblem, the aim is to make $y_t \rightarrow 0$ as fast as possible, subject to the constraint

$$|u_s + u_t| \leq 1 \tag{29}$$

Model Predictive Control (MPC) is an advanced technique of process control, in recent years it has also been used in power system balancing methods. MPC has the ability to anticipate future events can take control actions accordingly. Additionally for most of the advanced control methods a fast computation machine is required to execute their complex and time consuming calculation in real time. This is a big problem in the past as such computers were very costly and not easy to get.

MPC is the fact that it allows the current time slot to be optimized. This is achieved by optimizing a finite time horizon, but only implementing the current time slot. The most significant future that distinguishes MPC from other control algorithms is its long range prediction concept. The industry is now demanding a tighter advanced control strategy with the ability to integrate all the requirements to reduce operating costs, improve product quality, better use of energy resources and reduce environmental emission.

The optimization problem takes into account estimates of future quantities based on available information at each time step. The control policy involves feedback since real-time measurements are used to determine the control input. With RHC, an optimization problem is solved at each time step to determine a plan of action over a fixed time horizon. Analogous to the task of the exogenous Kalman filter, the plant Kalman filter is described by,

$$\tilde{x}^+ = A\tilde{x} + B_1\omega + B_2u + L_y(y - \tilde{y}) \tag{30}$$

$$\tilde{y} = C\tilde{x} + D_1\omega + D_2u \tag{31}$$

The overall settings of the suggested management criteria mixing the steady-state control u_s and the transient control u_t is shown in Figure 7.

3.2.1 ANFIS Controller Scheme

Adaptive Network based Fuzzy Inference System (ANFIS) is a neuro fuzzy technique where the combination is made between the neural network and the fuzzy inference system.

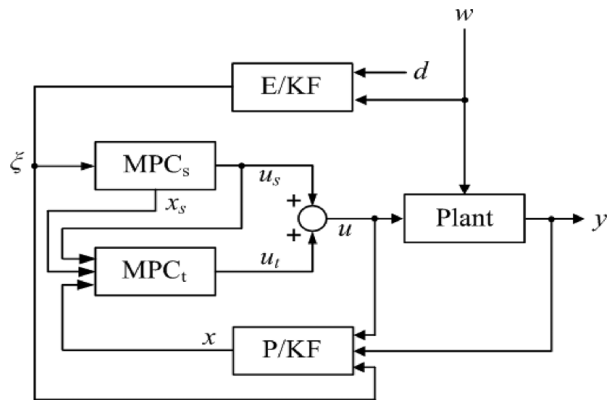


Figure 7. Complete MPC controller for the distributed generation inverter with exogenous and plant kalman filter.

In ANFIS the parameters can be evaluated in such a route, to the point that both the Sugeno and Tsukamoto fluffly models are spoken to by the ANFIS architecture. Again with minor imperatives the ANFIS model takes after the Radial Basis Function Network (RBFN) practically. This ANFIS strategy contains a mixture arrangement of fuzzy logic and neural network technique. The fuzzy logic considers the imprecision and instability of the framework that is being displayed while the neural system gives it a feeling of versatility.

Utilizing this half and half technique, at initial an introductory fuzzy model alongside its data variables are inferred with the assistance of the standards extricated from the information yield information of the framework that is being demonstrated. Next the neural system is utilized to tweak the standards of the beginning fuzzy model to deliver the last ANFIS model of the framework. In this proposed work ANFIS is utilized as the spine for the ID of true frameworks.

The benefit of the fuzzy inference system is that it can manage phonetic expressions and the upside of a neural system is that it can be prepared thus can self-learn and self-make strides. Jang (1993) took both points of interest,

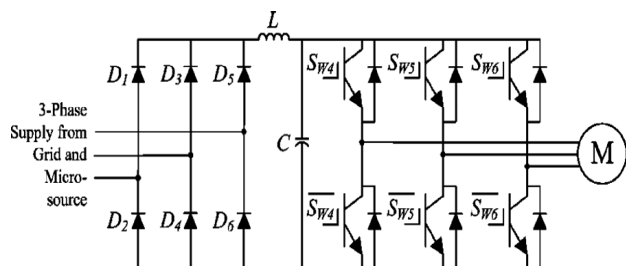


Figure 8. Structure of 15- KVA three phase adjustable speed drive.

joining the two procedures, and proposed the Adaptive Neuro-Fuzzy Inference System (ANFIS). It is computationally efficient and works well with linear techniques, optimization and adaptive techniques. It is well suited to mathematical analysis.

4. Simulation Results

The simulation model of the grid presented in Figure 1 is executed in Matlab/Simulink. The microgrid is proven under many conditions to calculate its capacities when operating linked and islanded from the distribution grid. There are three different load classes consisting of linear and nonlinear loads are designed. The per phase currents drawn by loads 1, 2 and 3 for $0 \leq t \leq 0.4s$ are shown in Figure 9.

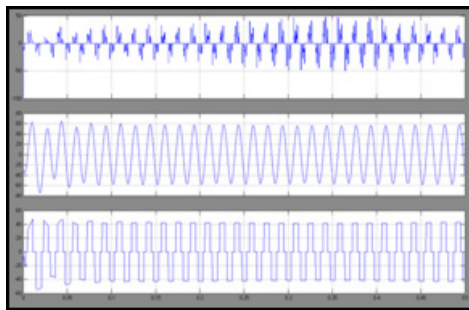


Figure 9. Per phase currents drawn by the three loads.

4.1 Proposed Method Results

Test Case 1: Power quality improvement with load-sharing during grid-connected operation.

The first test case indicates the capability of the microgrid to enhance the power quality of the distribution network by balancing for the harmonics in the total load current i_L due to the nonlinear loads that are joined to the distribution network, such that the harmonics will not propagate to the rest of the distribution network

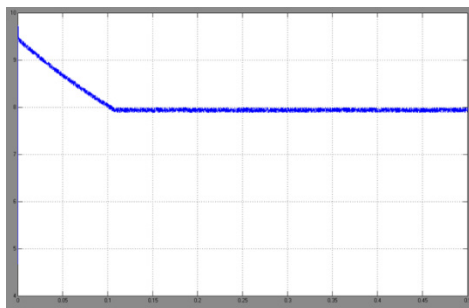


Figure 10. Waveform of the SB current for the time being charging.

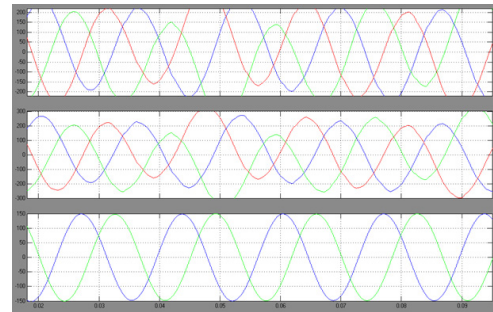


Figure 11. Waveforms of three phase load current (top), three phase distributed generation current (middle), and three phase grid current (bottom).

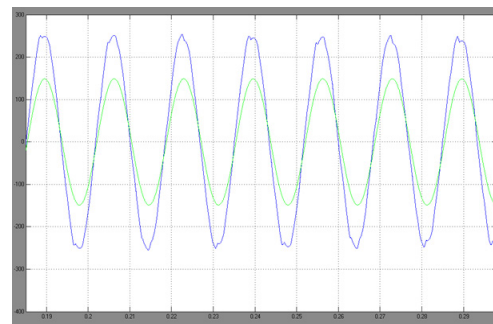


Figure 12. Waveforms of grid voltage and current for phase a.

during grid connected operation. The storage battery current I_b for $0 \leq t \leq 0.4s$ are shown in Figure 10.

The waveforms of the total load current i_L , the current supplied by the main DG unit i_{DG} and grid current i_g under this test case are shown in Figure 11. Figure 12 shows closed up waveforms of the grid voltage v_g and i_g of phase a. It is observed that the waveform of is in phase with that of with power factor improvement.

Test Case 2: Peak shaving of loads for the time being peak intervals.

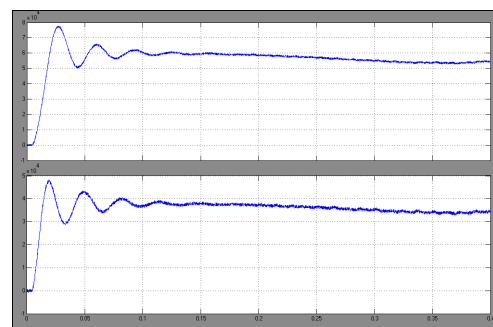


Figure 13. Active (top) and reactive (bottom) power absorbed by loads.

The second test case demonstrates the operation of the microgrid to achieve peak shaving in order to reduce the cost of generation from the grid. The waveforms of active and reactive power absorbed by loads, dispatched by the main DG unit and transported by the grid shown in Figures 13-15.

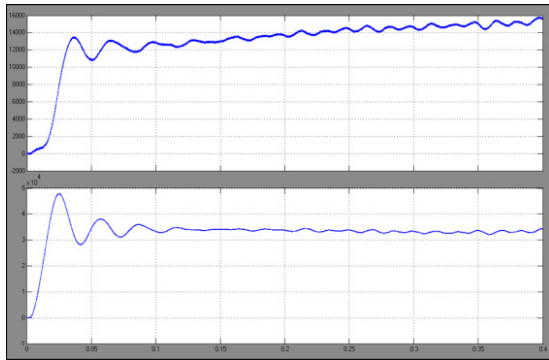


Figure 14. Active (top) and reactive (bottom) power dispatched by the main distributed generation unit.

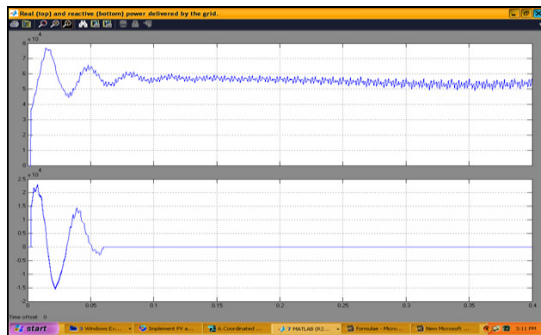


Figure 15. Active (top) and reactive (bottom) power transported by the grid.

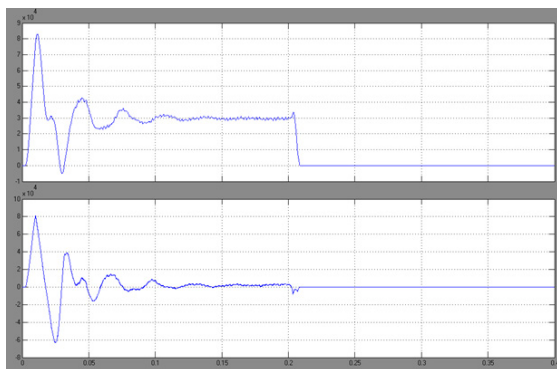


Figure 16. Active (top) and reactive (bottom) power dispatched by the grid.

Test Case 3: Load dropping amid islanded operation.

The third test case indicates the operation of the microgrid when it islands from the grid. In this test case, the microgrid is initially operating in the grid joined mode after 0.2s disconnected from the grid are shown in Figures 16 and 17.

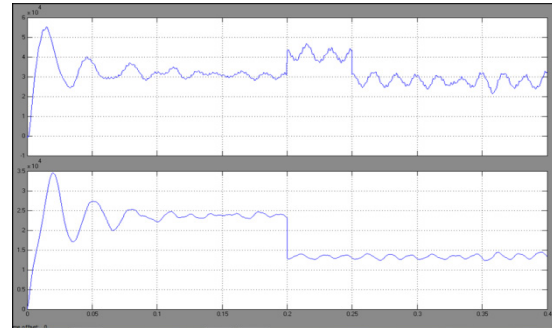


Figure 17. Active and reactive power delivered by the grid.

4.2 Extension Method Results with ANFIS

When ANFIS controller is used in place of MPC controller to minimize the disturbances and improve the stability of the system as shown in following Figures 18 to 23.

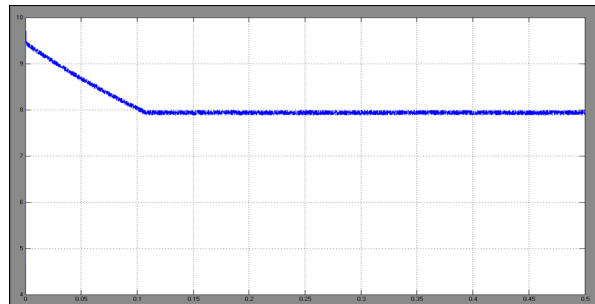


Figure 18. Waveform of the SB current in the course of charging.

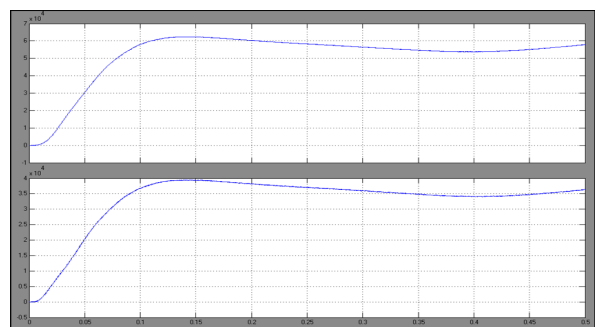


Figure 19. Real (top) and reactive (bottom) power received by loads.

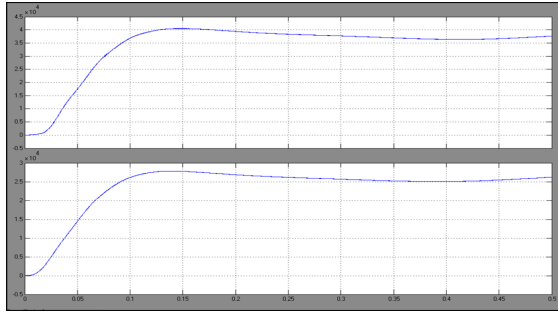


Figure 20. Real (top) and reactive (bottom) power dispatched by the main DG unit.

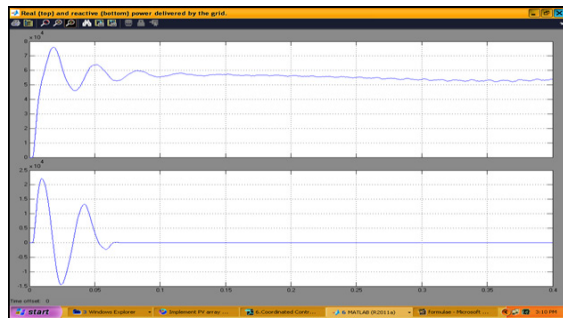


Figure 21. Real (top) and reactive (bottom) power transferred by the grid.



Figure 22. Real (top) and reactive (bottom) power dispatched by the grid.

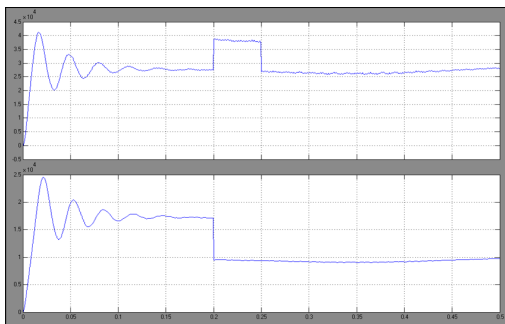


Figure 23. Real (top) and reactive (bottom) power received by the loads.

5. Conclusion

In this framework, a control plot that orchestrates the capacity of a few DG inverters in a microgrid for lattice joined and islanded highlights have been given. To recognize the acute lines regard, distinct strength administration highlights, for example, ideal cutting and burden shedding have in the same way been as well in the test system research. The results have checked that the microgrid has the capacity manage distinctive working circumstances effectively amid network joined and islanded highlights, subsequently enhancing the general dependability and solidness of the microgrid. In extension perform flexible neuro fuzzy control criteria for interfacing inverter is included. The operator performs satisfactorily under the dynamic working circumstances. It has also been proven that the inverter is able to execute all the responsibilities of the shunt APF while keeping the smooth bidirectional power flow at the same time.

6. References

1. Ezhilarasan S, Palanivel P, Sambath S. Design and development of energy management system for DG source allocation in a micro grid with energy storage system. *Indian Journal of Science and Technology*. 2015 Jun; 8(13):58252.
2. Hatzigiargyriou N, Asano H, Iravani R, Marnay C. Micro grids: An overview of ongoing research development and demonstration projects. *IEEE Power and Energy Magazine*. 2007 Aug; 5(4):78–94.
3. Geetha R, Jayachitra V. Simplified reactive power control for grid-connected photovoltaic inverters. *Indian Journal of Science and Technology*. 2015 Jul; 8(13):57487.
4. Nayagam VS. Power reliability improvement of inverter with photovoltaic system. *Indian Journal of Science and Technology*. 2015 Mar; 8(6), 570–3.
5. Mohamed A. Micro grid modeling and online management [PhD thesis]. Helsinki, Finland: Helsinki University of Technology; 2008.
6. Sultana WR, Sahoo SK, Kiran KS, Reddy GTR, Reddy PH. Predictive control of three-phase cascaded multilevel inverter. *Indian Journal of Science and Technology*. 2015 Jan; 8(S2):45–9.
7. Mattingley J, Wang Y, Boyd S. Receding horizon control: Automatic generation of high speed solvers. *IEEE Control Syst Mag*. 2011 Jun; 31(3):52–65.
8. Moreno V, Pigazo A, Diego RI. Reference estimation technique for active power filters using a digital Kalman algorithms. *Proceedings of International Conference Harmonics Quality of Power*; 2002 Oct 6-9. p. 490–4.